ISSN 1345-3041

VOL. 94/JUN. 2001

MITSUBISHI ELECTRIC ADVANCE

Automobile-Human Technology Edition

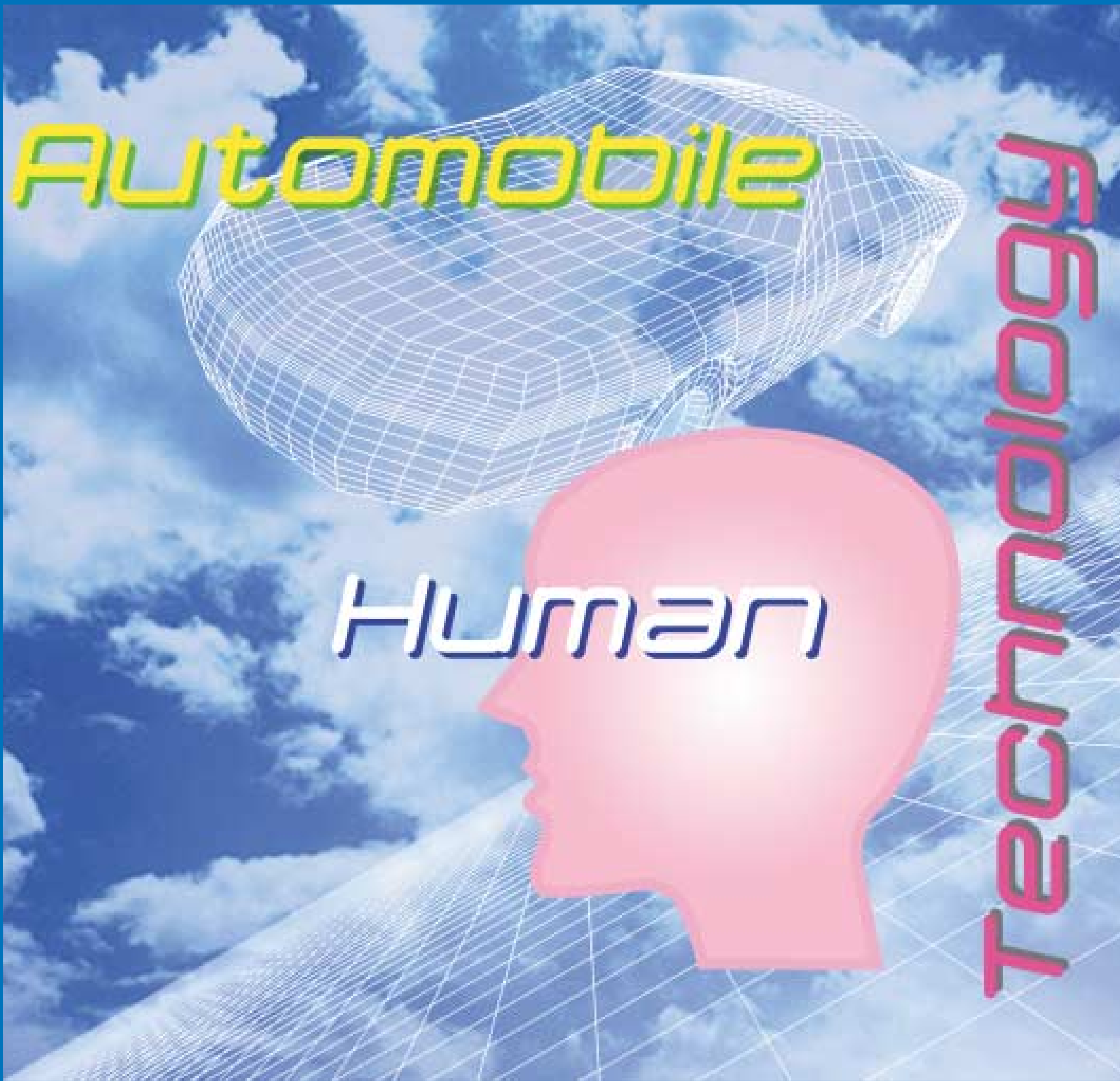

MITSUBISHI ELECTRIC

A Quarterly Survey of New Products, Systems, and Technology

●Vol. 94/June 2001 Mitsubishi Electric **ADVANCE**

Automobile-Human Technology Edition

CONTENTS

Technical Reports

Cover Story

Our cover expresses a world in which globalization is accompanied by environmental protection under clean, clear blue skies. Mitsubishi Electric seeks to achieve harmony in the links between human beings and the automobile, developing the advanced technology that addresses the informational, environmental and safety concerns.

Editorial Inquiries

Keizo Hama
Corporate Total Productivity Management & Environmental Programs
Mitsubishi Electric Corporation
2-2-3 Marunouchi
Chiyoda-ku, Tokyo 100-8310, Japan
Fax 03-3218-2465

Product Inquiries

Yasuhiko Kase
Global Strategic Planning Dept.
Corporate Marketing Group
Mitsubishi Electric Corporation
2-2-3 Marunouchi
Chiyoda-ku, Tokyo 100-8310, Japan
Fax 03-3218-3455

Mitsubishi Electric Advance is published on line quarterly (in March, June, September, and December) by Mitsubishi Electric Corporation.

Overview

Advanced Technologies for Man/Automobile Harmony

*by Masaaki Nangaku**

The automobile, while comfortable and convenient for its users, causes a number of serious problems, such as pollution of the atmosphere and other environmental and energy-related problems. There are also the risks of traffic accidents and other safety-related problems. The solutions of these problems are some of the most important issues facing us in the 21st century. Only advances in technology offer the prospect of solutions, and we need nothing less than a complete paradigm shift.

We at Mitsubishi Electric Corporation take "man/automobile harmony" as our watchword, and we are actively applying information technology (IT) to advanced developments in environmental and energy-saving technology, and in safety, convenience and comfort. In this way we intend to contribute to progress in our automotive culture.

While these technological developments naturally include the whole spectrum from miniaturization and weight reduction to sophisticated electronic control technology, they also call for complex and rapid development of communication, information-processing and semiconductor technologies.We will also see rapid progress in the modularization and systemization of automotive electronic products.

Fortunately, the corporation has excellent, in-depth resources and achievements in each of these areas, and by utilizing and integrating these different disciplines we expect to be able to take up successfully the challenges of creating a new automotive culture appropriate for the needs of the 21st century, at the same time contributing to the economic development of society.❑

**Masaaki Nangaku is Senior Executive Vice President and a Member of the Board of Mitsubishi Electric Corporation.*

Application of CFD Analysis to the Development of a Direct-Injection System

*by Hideaki Katashiba and Kazuhiko Kawajiri**

Direct-injection gasoline engines have been widely introduced in global markets in recent years as environmentally friendly engines. To improve their fuel economy and low-emission performance further, it is necessary to have a better understanding of the fuel spray pattern, mixture formation and combustion state in the cylinder so that fuel supply control and component characteristics can be optimized. This article describes a computational fluid dynamics (CFD) analysis method that has been applied to ascertaining these in-cylinder conditions and presents the results of basic experiments conducted during the development process.

Fuel Spray Model

The behavior of fuel injected directly into the cylinder is a major factor governing mixture formation. A fuel spray model capable of calculating fuel spray behavior accurately must be developed in order to calculate the mixture formation process. In the CFD analysis, in-cylinder gas flow was found by applying the finite element method to solve equations for the mass and momentum of a compressible fluid and the equation for conservation of energy. The standard k-ε turbulence model was used. Fuel spray behavior was calculated based on a discrete droplet model, taking into consideration droplet break-up, coalescence and evaporation. The initial spray condition was given as a function of the plunger operation, including the initial injection velocity, injection angle and droplet size that were determined from the injector specifications. These values were then corrected based on a comparison with the results of experimental measurements of fuel spray properties. The gasoline fuel was assumed to be C_8H_{18} and its physical properties were used in the analysis. The distribution function proposed by Nukiyama and Tanasawa was assumed for the initial droplet size distribution.

The simulation results obtained with the fuel spray model developed in this study are compared in Fig. 1 with the experimental results for fuel spray growth when fuel was injected under a backpressure condition of atmospheric pressure. The experimental results are shown as images captured with a high-speed camera fitted with a photomultiplier. These images are cross-sections of the fuel spray that were visualized by means of an Ar laser light sheet. The simulation results show overall images of the fuel spray. It is clear from this figure that the newly developed fuel spray model accurately reproduced fuel spray growth behavior. Fig. 2 compares the experimental and simulation results for spray penetration and the spray cone angle.

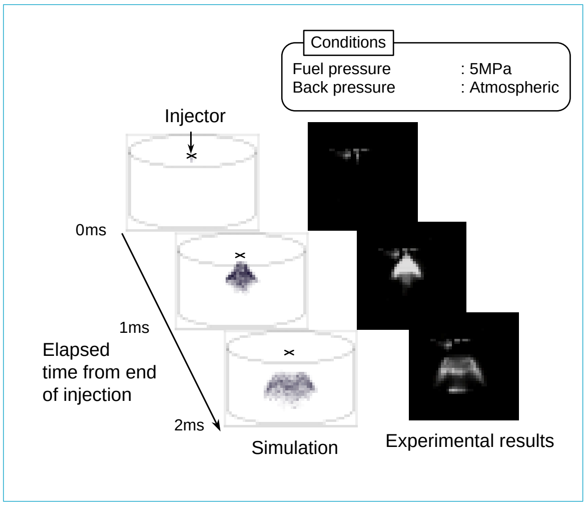

Fig. 1 Simulation results for fuel spray growth.

Good agreement is seen between the two sets of results for both spray penetration and the spray cone angle. It was also confirmed that the experimental and simulation results showed good agreement with respect to the Sauter Mean Diameter of the spray droplets following injection.

In-Cylinder Mixture Formation

Visualization of in-cylinder mixture formation by simulation allows quantitative evaluation of the phenomena involved, which is a critical factor in designing the optimum fuel injection system. In stratified-charge combustion, it is necessary to make effective use of the cavity provided at the top of the piston to transport a compact combustible mixture cloud to the vicinity of the spark plug for ignition and combustion. In this study, an analysis was made of the

**Hideaki Katashiba is with Automotive Electronics Development Center and Kazuhiko Kawajiri is with Advanced Technology R&D Center.*

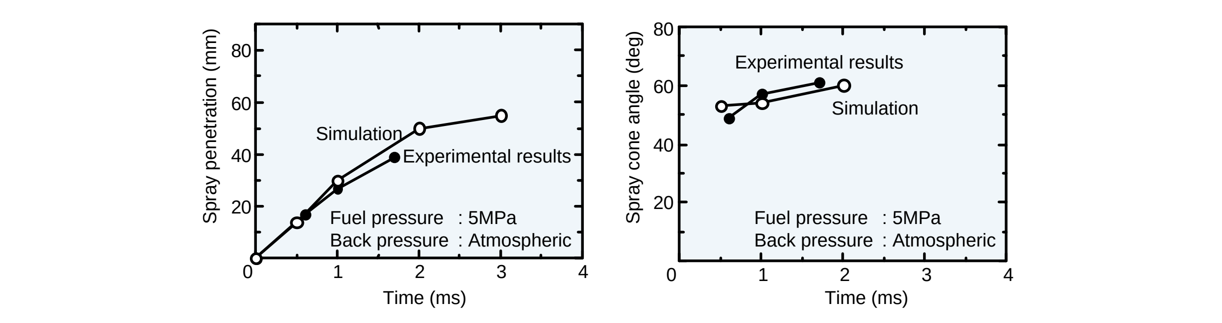

Fig. 2 Spray penetration and spray angle obtained in fuel injection simulation.

influence of the fuel spray angle produced by the injector, which represents a key engine component, on mixture formation in the cylinder.

The configuration of the combustion chamber of the direct-injection gasoline engine that was analyzed is shown schematically in Fig. 3. The injector was positioned between the two intake ports, and fuel was injected at an oblique angle toward the eccentric piston cavity. The spark plug was centrally located at the top of the cylinder. Calculations were performed for three types of initial spray cone angles of 50°, 60° and 70° and the spray behavior was compared.

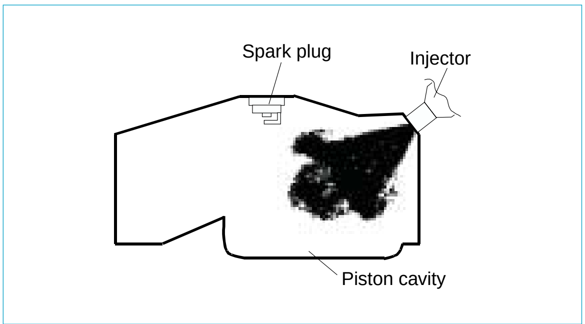

Fig. 3 Combustion chamber of direct injection gasoline engine.

Fig. 4 compares the fuel spray behavior in the combustion chamber. With a spray cone angle of 70°, the broad spray pattern causes the fuel to overflow the cavity, with the result that a

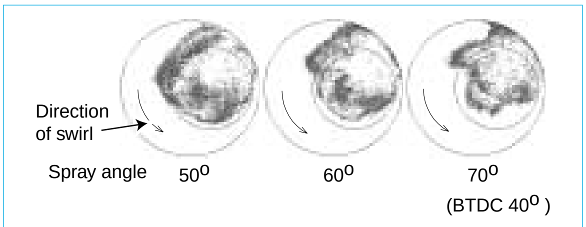

Fig. 4 Behavior of fuel spray in combustion chamber.

large quantity of fuel sticks to the walls. It is estimated that a larger quantity of unburned fuel would be evacuated from the cylinder under this condition. With a small spray cone angle of 50°, many spray droplets overflow the cavity following collision with the piston top surface, resulting in a short interval for obtaining the optimum A/F ratio. As described here, simulations allow the spray behavior and mixture distribution to be estimated, making it possible to design the optimum fuel spray properties and other parameters.

Combustion Simulation

This section describes the combustion simulation program that was developed for making detailed visualizations and evaluations of complex combustion phenomena in the cylinder and presents an example of the simulation results. This combustion simulation technology is based on the combustion analysis expertise that we have accumulated over many years in connection with fan heaters, furnaces and the like. Combustion reactions were assumed to be single-stage irreversible reactions. A flame area progression model was used as the combustion model, which assumed that combustion proceeded by means of an advancing of a thin-flame front in the combustible mixture. The mean propagation velocity of the flame front ω is given by the following equation, assuming that it is proportional to the spatial gradient of the turbulent combustion velocity S_t and the unburned mass fraction m_{fu}.

$$\omega = C_r \rho_u S_t |\nabla m_{fu}| \quad \text{Eq. (1)}$$

$$S_t / S_u = 1 + C_s u' / S_u \quad \text{Eq. (2)}$$

where ρ_u is the density of the unburned gas, S_u is the laminar burning velocity, u' is the turbulence intensity and C_r and C_s are constants.

The simulation results for flame propagation behavior in the cylinder during homogeneous-charge combustion are compared in Fig. 5 with the experimental data. A single-cylinder optical engine having the piston head and part of the cylinder liner made of quartz glass was used in the experiments to visualize in-cylinder combustion phenomena by means of a high-speed camera fitted with a photomultiplier. The simulation results are shown only for the visualized region relative to the piston diameter. As shown in the figure, the simulation reproduced flame propagation behavior with excellent accuracy as a result of suitably adjusting the model constants used in the combustion model.

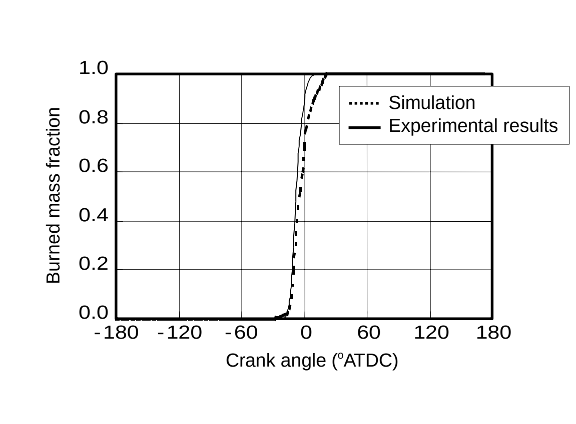

Fig.7 Simulation results of burned mass fraction.

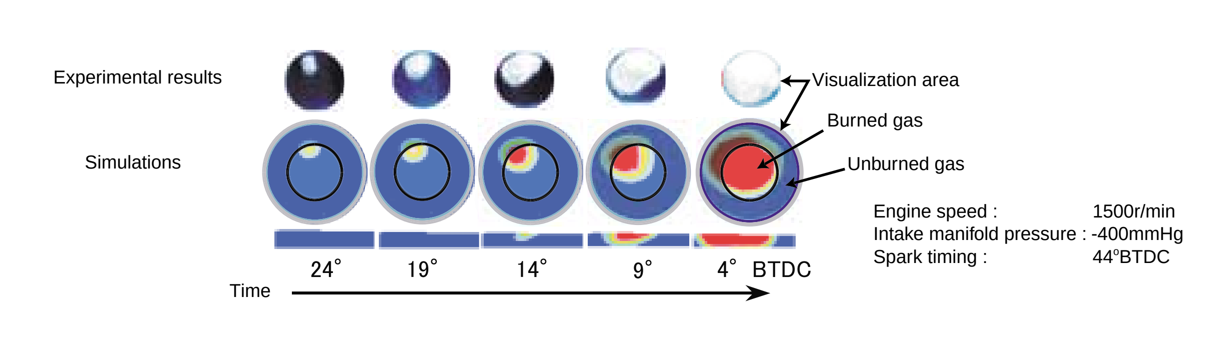

Fig.5 Behavior of flame propagation.

The newly developed combustion model was then applied to an analysis of stratified-charge combustion. The simulation results for cylinder pressure and burned mass fraction are compared with the experimental data in Figs. 6 and 7, respectively. Although the peak combustion pressure calculated in the simulation was several percentage points higher than the experimental value, the simulation results for cylinder pressure and burned mass fraction show good overall agreement with the experimental data. As indicated here, the newly developed combustion model can be applied to combustion calculations for a direct-injection gasoline engine, making it possible to ascertain combustion phenomena and to utilize the resulting data in engine design studies.

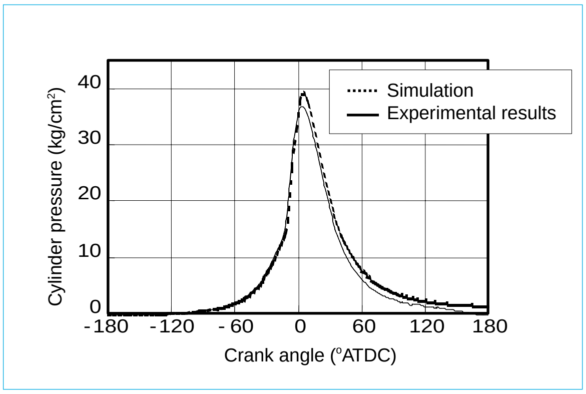

Fig.6 Simulation results for cylinder pressure.

In future work, this simulation technology will be applied to the development of next-generation direct-injection engines and their components with the aim of contributing to the creation of products that achieve even higher fuel economy and lower exhaust emissions.❑

Application of a GMR Element to a Revolution Sensor

*by Tatsuya Fukami and Masayuki Ikeuti**

A giant magnetoresistive (GMR) element, having a signal amplitude one order of magnitude larger than a conventional semiconductor Hall element, has been successfully applied to a revolution sensor for automotive use for the first time in the world. Featuring an original signal-processing IC and a monolithic structure, this sensor achieves a high signal-to-noise (S/N) ratio to facilitate sophisticated sensing applications such as detection of engine misfire.

Revolution sensors for automotive applications are typically used in controlling the engine, brakes and automatic transmission. Sensors employed for engine control in particular must provide high-temperature stability at temperatures above 150°C. In just ten years since the discovery of the GMR effect, with its large magnetoresistance ratio, GMR elements have been applied to magnetic heads, magnetic field sensors and other devices. However, their application to automotive sensors, which must be usable at high temperatures, has lagged behind their application to other devices. This is attributed to a problem with the long-term stability of the GMR film in a high-temperature environment. Our objective was to improve the high-temperature stability of the GMR element by annealing it beforehand under suitable conditions.

The GMR film we fabricated is a multilayer film produced by repeatedly depositing a magnetic layer, consisting mainly of Co, and a nonmagnetic Cu layer. The GMR film composition, including the magnetic layer thickness and Cu layer thickness, was optimized so as to achieve a large magnetoresistance ratio and the smallest possible hysteresis.

Magnetoresistance curves measured for GMR films following annealing for ten hours at different annealing temperatures are shown in Fig. 1. Letting Rmin + DR and Rmin express the maximum and minimum magnetoresistance values in the range of the measured magnetic field, the magnetoresistance ratio is DR/Rmin. As shown in Fig. 1, the magnetoresistance ratio increased until an annealing temperature of 250°C. However, at an annealing temperature of 300°C, not only did the magnetoresistance ratio decline sharply, the saturation magnetic field and magnetic hysteresis increased, resulting in characteristics that are not suitable for a sensing element. Judging from the desirable sensing characteristics, an annealing temperature range of 200°~250°C would be optimum. However, in consideration of the harsh temperature environment of automobiles, 250°C was selected as the annealing temperature because of the higher thermal stability that can presumably be obtained. The magnetoresistance ratio achieved following annealing at this temperature is a high 34% and hysteresis is also low, thus exhibiting excellent characteristics for a sensing element. Fig. 2 shows the long-term high-temperature stability measured at 170°C for a GMR element that was annealed for ten hours at 250°C. The vertical axis shows the rate of change in the magnetoresistance ratio and from the smallest initial value. After 2,000 hours, the rate of

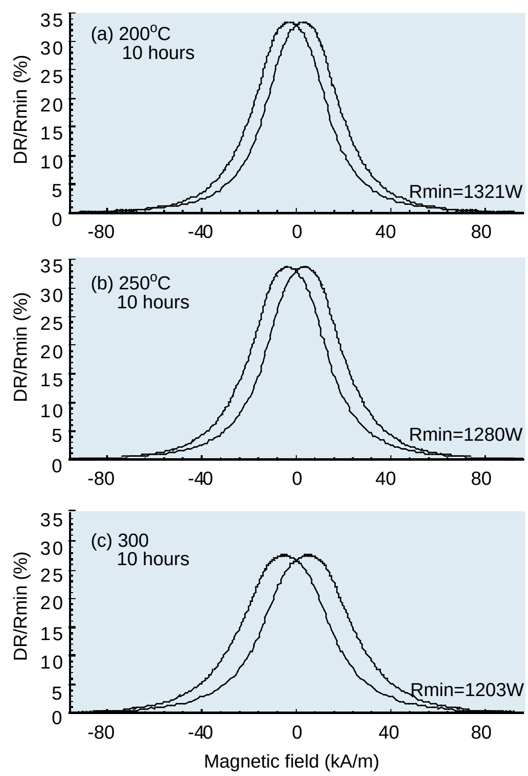

Fig. 1 MR curves after 10 hours annealing.

Tatsuya Fukami is with Advanced Technology R&D Center and Masayuki Ikeuti is with Himeji Works.

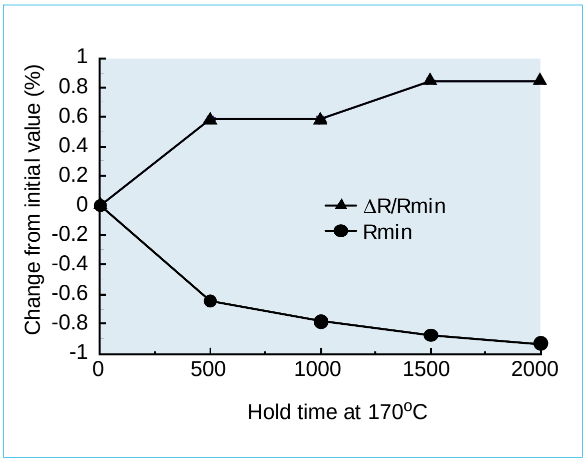

Fig. 2 Long term stability test at 170°C.

change in the magnetoresistance ratio and from the smallest value was less than 1%, which is sufficiently small. These results show that the GMR element has sufficient thermal stability for use as an automotive sensor.

With the aim of reducing noise, we then examined the possibility of integrating a GMR element with a signal processing IC on a monolithic chip. To achieve a monolithic structure, it is necessary to deposit the GMR element after the IC has been fabricated, taking into account the thermal resistance of the GMR element. The issue here is how to use the phosphate-silicate glass (PSG) film, which serves as the insulator of the signal processing IC, as the GMR substrate in order to obtain excellent GMR properties. The PSG film has large surface roughness, making it unsuitable as the GMR substrate. It was found that excellent properties can be obtained by ion-beam etching (IBE) the PSG film surface for at least two minutes before depositing the GMR film. It is thought that IBE has the effect of cleaning the insulator surface that becomes dirty during the fabrication process and simultaneously smoothing large surface irregularities.

The revolution sensor for automotive application consists of the newly developed monolithic IC chip, a permanent magnet and components for protection against surge current (Fig. 3). This sensor measures the rotation of gears made of a soft magnetic material. The gear teeth made of a soft magnetic material are magnetized when they approach the permanent magnet. Because the magnetized teeth cause the GMR element to produce a magnetic field, a magnetic field that changes with gear rotation is applied to the GMR element. The changing magnetic field applied to the GMR element causes the electrical resistance of the element and also the voltage between the two terminals to vary. The voltage change is amplified and then compared by the signal-processing circuit, which converts gear rotation into a digital electrical signal, making it possible to detect the edge of the gear.

The above-mentioned characteristics of this revolution sensor were evaluated using a standard-shaped gear. Measurement accuracy was given by the deviation in the output timing of the revolution sensor relative to a high-accuracy encoder signal (reference signal) used to monitor gear rotation. As the first step, the same measurement was performed at different measurement temperatures, Ta. The gear was rotated at a speed of 7,000rpm, and the distance between the sensor and the gear was kept con-

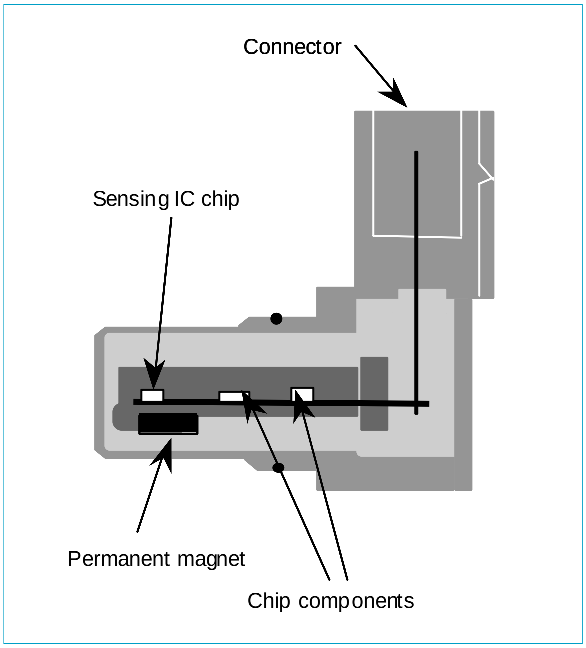

Fig. 3 Structure of the revolution sensor.

stant at d = 1 mm. As shown in Fig. 4, the evaluated sensor provided excellent angle detection accuracy to within ±0.26° over a wide temperature range (–40° C ≤ Ta ≥ 145° C), which is one operating requirement of a revolution sensor for automotive applications.

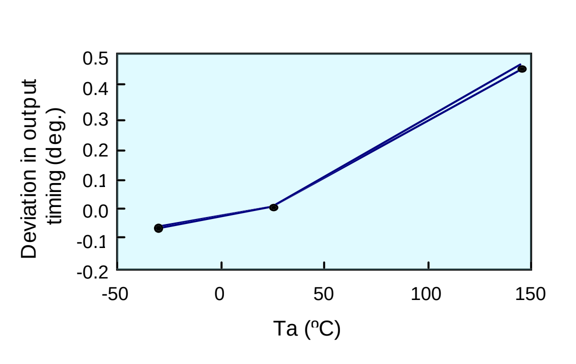

Fig. 4 Temperature dependence of output timing.

An evaluation was then made of sensor repeatability, which is a key parameter of the misfire detection performance of a sensor intended for use in engine control. Repeatability is an index that shows the dispersion of the edge position in the sensor output signal while a gear is rotating. It is defined as the maximum rotational speed dispersion when a gear is subjected to repeated rotation tests. In order to detect engine misfire, a sensor must have sufficient accuracy to detect minute changes in rotational speed, which requires exceptionally good repeatability. Fig. 5 shows the results of repeatability measurements made at different rotational speeds under harsh conditions of d = 1.5mm and Ta = 145° C. Nearly a flat characteristic was obtained at all rotational speeds. The timing differed slightly depending on the gear teeth, but this was caused by timing fluctuation due to sensor noise induced by external interference. This fluctuation is sufficiently small, being about one-third that of a semiconductor Hall revolution sensor. This reduction of noise has resulted from the use of a GMR element, which provides a signal amplitude that is an order of magnitude larger, and the integration of the GMR element and signal processing circuit on a monolithic chip.

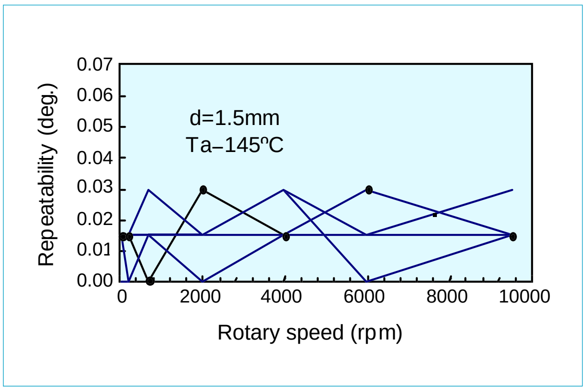

Fig. 5 Rotary speed dependence of repeatability.

The measured results show the enormous potential of the monolithic GMR sensing element for various applications, including its capability for detecting engine misfire, which was previously impossible with conventional devices.❑

On-Board Inverter Miniaturization Technology

*by Hirotoshi Maekawa and Gourab Majumdar**

In recent years, hybrid electric vehicles (HEVs) that combine conventional internal combustion engines and electric motors have come into the spotlight as cars that can both improve fuel efficiency and reduce exhaust gases. This article discusses the development at Mitsubishi Electric Corporation of technologies that are used in inverter equipment-a key part of any HEV-and, in particular, discusses the development of technologies for miniaturizing inverters.

Technologies for Miniaturizing On-Board Inverters

Two major issues to be overcome in miniaturizing inverter equipment for use with high voltages and large electric currents are the handling of both inductive noise and the heat generated through power losses within the elements. If the inverter is to be used in the demanding on-board environment found in vehicles, the equipment must also be resistant to physical shocks, thermal shocks and power cycling. The equipment must provide high reliability under these severe conditions, so such inverters require more exacting technical innovations than inverters for general use.

Fig. 1 shows a cross section of an on-board inverter integrated intelligent power-drive unit (IPU) currently under development. Advances in miniaturization have required design innovations in a variety of areas. Three key technologies contributing to the miniaturization of the power inverters are discussed below.

POWER CHIPS. Because power chips play a critical role in controlling the performance of the inverter equipment, improvements to the power chips have long been a focus of development at Mitsubishi Electric.

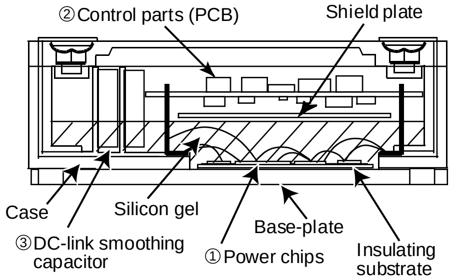

Fig. 1 Structure cross section.

The power semiconductor element, known as the insulated gate bipolar transistor (or IGBT) or the free-wheeling diode (FwDI), is a critical component of the inverter equipment. While the top priorities in the development of the power semiconductor elements at the corporation are those of miniaturizing the elements and reducing power losses, efforts are simultaneously directed at reducing electromagnetic interference and noise.

For IGBT chips, Mitsubishi Electric has pioneered the successful advance of microelectronic processing from the conventional third-generation process rule technologies (three-micron level) to the fifth-generation (submicron level) using planar-type IGBTs, taking advantage of the track record these IGBTs have in on-board applications.

By implementing these advanced microelectronic processes, the corporation has succeeded in increasing current densities significantly, from $130A/cm^2$ to $200A/cm^2$ or more, making it possible to reduce the surface area of the chip by about 30%.

Fig. 2 shows the tradeoff frontier between saturation voltage and turn-off time for several generations of IGBTs. Compared with third-generation IGBTs, which are prevalent today, Mitsubishi Electric has succeeded in reducing the saturation voltage by 0.5V to 0.6V.

The benefits of this process technology are as follows:

1. The saturation voltage is reduced through the excellent performance of metal-oxide-semiconductor structures (MOS) fabricated using sub-micron fabrication technologies.

2. The saturation voltage is also reduced by optimizing the distribution of carriers within the IGBT using lifetime control.

3. FwDI soft recovery is enabled through the combination of heavy-metal distribution and local-lifetime control.

**Hirotoshi Maekawa is with Automotive Electronics Development Center and Gourab Majumdar is with Power Device Division.*

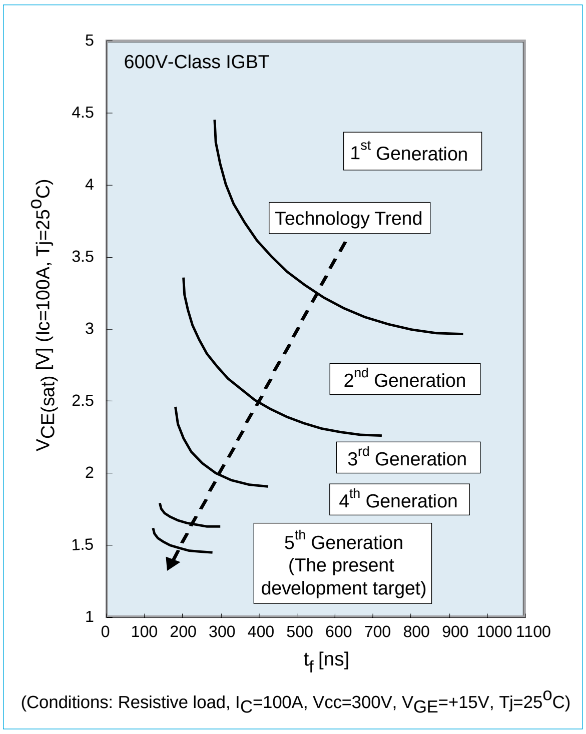

Fig. 2 $V_{CE(sat)}$ - t_r Trade-Off

Fig. 3 shows a comparison of the cross sections of a conventional FwDI diode and the newly developed FwDI diode. Because the percentage of time that the energy-recovery mode is used in HEV systems is relatively high, improvements in performance of the FwDI are critical. By locally shortening the lifetime of holes in the shaded region of the diagram, Mitsubishi Electric has succeeded in controlling the injection of holes to levels lower than conventional products, and doing so without sacrificing the voltage drop in the forward direction.

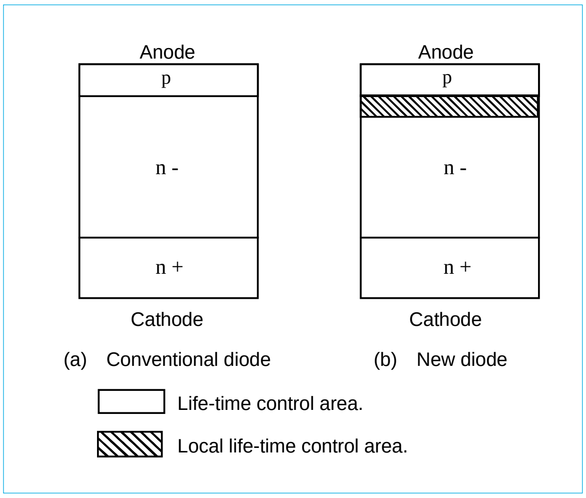

Fig. 3 Free-wheeling-diode (FwDi) cross-section structure comparison.

THE CONTROL CIRCUITRY. For the control circuitry, Mitsubishi Electric has succeeded in creating ultra-dense packaging that combines on a single circuit board the predrive circuits (such as the power-supply circuit to the power unit), the failure diagnostic circuits, and the high voltage power-supply sensors, along with the IGBT drive flash-protection circuits.

Newly-developed sheet-type transformers are used in the power unit power-supply circuitry, enabling a low-profile, compact shape.

Although push-pull circuits have been configured in the past using conventional transistor elements in the IGBT drive buffer elements, a switch to MOSFET elements reduces heating and allows for smaller IGBT driver circuits overall.

The IGBT protection circuit is a newly developed custom IC that combines on a single chip a variety of functions such as over-heat protection functions and gate voltage short-circuit functions using on-chip temperature sensors, in addition to providing conventional short-circuit protection functions. This custom IC integrates the IGBT gate-drive circuit and all of the its various peripheral protection circuits, allowing the IGBT peripheral circuitry to shrink substantially.

The CPU also uses a variety of sensors in gathering information and making adjustments, not only making it unnecessary to perform manual adjustments or to sort and match the electronic components but also making it possible to structure control circuits with the bare minimum number of electronic components. It does this by incorporating the functions of the logic circuit in software rather than hard-wiring them.

THE SMOOTHING CAPACITOR. At present, most vehicle-mounted inverter equipment uses aluminum electrolytic capacitors as the primary DC power-supply smoothing capacitors; unfortunately, these capacitors account for a relatively large percentage of the volume and weight of the inverter equipment as a whole, and have been a major impediment to miniaturization.

At Mitsubishi Electric, we have focused on the fact that the primary circuit power supply for the vehicle-mounted inverters is always the DC power-supply battery, and have thus engaged in development projects focused on reducing impedance in the high-frequency domain rather than using capacity as the selection criterion for the smoothing capacitor. Because of this, we have been able to set the goal of implementing a solid capacitor with a volume that is about one tenth that of a conventional capacitor.

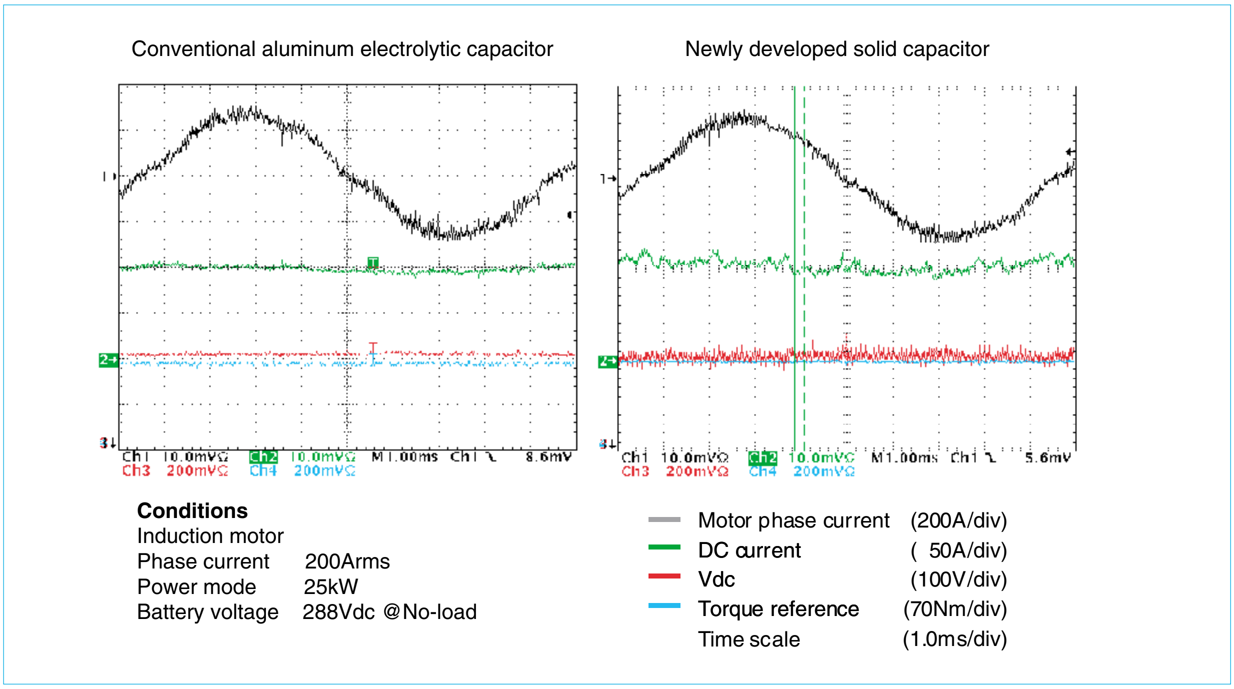

Fig. 4 Experimental Inverter Drive Waveforms Comparison.

The benefits of the solid capacitor currently used by the corporation are as follows:

1. It is small, light, and has a three-dimensional shape that does not take up excess space.

2. Its equivalent series resistance (ESR) and its impedance in the high-frequency domain are low.

3. It has all of the environmental characteristics required for on-board use, with a broad range usable temperature, a long life expectancy, and a high breakdown voltage.

Because the capacitor itself is smaller when the solid component is used, it can be positioned closer to the power element, with the additional benefit of allowing the power element itself to be smaller (optimizing the breakdown voltage) because of the snubber effect.

The smoothing capacitor is used to reduce the ripple from the DC power supply. The capacity required in the smoothing capacitor is determined by factors such as the type of battery, the inductance in the primary power-supply circuit, and the control software. In this development project, Mitsubishi Electric has worked to minimize the required value for the capacitance to control the voltage spike when the IGBT shorts. Fig. 4 shows the waveform when the motor is driven with the lowest capacitance value. This figure indicates that the new capacitors have characteristics in no way inferior to those of conventional aluminum dielectric capacitors.

The article describes technologies currently under development by Mitsubishi Electric for miniaturizing on-board vehicle-mounted inverters, one step in the corporation's efforts to develop smaller inverters with higher performance and so to contribute to the spread of environmentally friendly vehicles.❑

Millimeter-Wave Radar Technology for Automotive Application

*by Shinichi Honma and Naohisa Uehara**

Mitsubishi Electric Corporation has developed a millimeter-wave radar for automotive application. Monolithic microwave integrated circuits (MMICs), developed specifically for this application by Mitsubishi Electric, are used for the radio-frequency (RF) module to obtain outstanding radar performance. This millimeter-wave radar incorporates a signal-processing unit in the radar head, resulting in a more compact, lightweight radar system that is easy to install on vehicles.

The sensors for monitoring vehicle driving environments embody important technology for the Intelligent Transport System (ITS). Sensing devices employed include the ultrasonic sensor, image-processing sensor, infrared lidar, microwave radar and millimeter-wave radar. Compared with other types of sensors, a millimeter-wave radar has the advantage of providing stable detection of targets even under inclement weather conditions such as rain or snow. Recent remarkable advances in RF technology have facilitated production of highly functional and efficient radar sensors. Thus, millimeter-wave radar has been marketed as, a vehicular collision warning sensor.

The RF technology, semiconductor technology and radar technology that Mitsubishi Electric has developed over many years for space, defense and consumer electronics applications have been used to create a millimeter-wave radar for use on vehicles. One of the features of this radar is that all of its constituent elements, including the semiconductor devices, have been developed in-house specifically for automotive radar application.

Measuring Distance and Velocity

The method of measuring the distance from a radar to a target vehicle and the vehicle's relative velocity depend on the type of radar system employed. Millimeter-wave radar systems for automotive application include pulse radar, frequency-modulated continuous-wave (FM-CW) radar and spread spectrum radar. The newly developed millimeter-wave radar is based on the FM-CW radar system.

The FM-CW radar system allows a simple construction of the RF circuit. Moreover, this system has often been adopted for automotive millimeter-wave radars because it can measure both the distance to a target and the target's relative velocity simultaneously. The measurement principle of the FM-CW radar system is shown in Fig. 1. The radar transmits a frequency-modulated millimeter-wave signal, and the signal reflected by a target is received by the radar. By mixing the received and transmitted signals, the system obtains a beat signal having a frequency of f_b. This beat signal features a time-delay due to the distance from the radar to the target and a Doppler shift due to the relative velocity of the target. The range to the target, R, and its relative velocity, V, are found with the following equations using the pair of beat signal frequencies, f_{b1} and f_{b2}. These beat signals are obtained from the pair of frequency-modulated waves having different time variations.

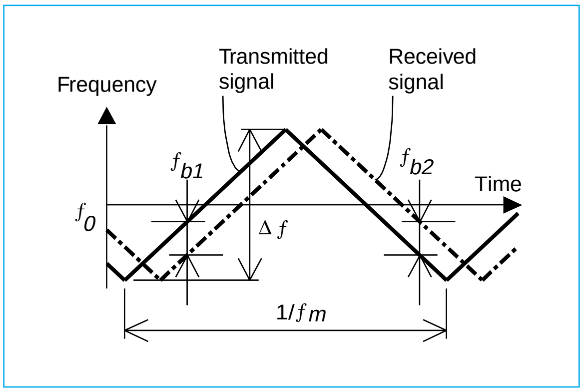

Fig. 1 Frequency-time relationships in FM-CW radar.

$$R = \frac{(f_{b1} + f_{b2})c}{8 f_m \Delta f} \quad \text{(Eq. 1)}$$

$$V = \frac{(f_{b2} - f_{b1})c}{4 f_0} \quad \text{(Eq. 2)}$$

where c is the velocity of light, f_0 is the center frequency, f_m is the modulation frequency and Δf is the maximum frequency deviation.

*Shinichi Honma and Naohisa Uehara are with the Automotive Electronics Development Center.

When two or more targets and objects exist, the beat signals obtained from them have multiple frequency components. Consequently, in order to detect the distance to a target and its relative velocity accurately, it is essential to select the pair of beat signals from the same object without error. In order to use a millimeter-wave radar as the sensor for an adaptive cruise control (ACC) system or an automated driving system, it is necessary to reduce the target misrecognition rate as much as possible.

Masuring the Azimuth

The monopulse method illustrated in Fig. 2 is often used to measure target azimuth. The reflected signals from the same target are received as two beams having different directions. The azimuth is determined according to the following procedure from the received field intensity of the two beams.

1. The difference and the sum of field intensities for the two beams are obtained for each angle. A discrimination curve that shows the relationship between the angular-error signal voltage ε and the azimuth θ is obtained. The angular-error signal voltage is obtained by normalizing the difference signal with the sum signal.

2. The reflected signals from the same target are received as two beams having field intensities of α and β. The difference δ between these two intensities, and their sum σ, are then calculated.

3. For these pairs of field intensities, the ratio of the difference to the sum (δ/σ) is compared with the angular-error signal voltage of the discrimination curve. And then the azimuth θ_t of the target is uniquely identified.

Table 1 Technical Specification of the Millimeter-wave Radar.

Item	Performance
Frequency	76 ~ 77GHz
Output power	10mW max
Range	0 ~ 120m (Passenger car)
Range resolution	1m
Relative speed	-100 ~ +200km/h
Speed resolution	1km/h
Detection angle	±8deg.
Multiple target detection	Possible
Data refresh rate	100msec

In order to obtain two beams, a sequential lobing method is adopted in this radar for automotive use. For this purpose, a mechanical scanning method with an antenna radiating a single beam is adopted.

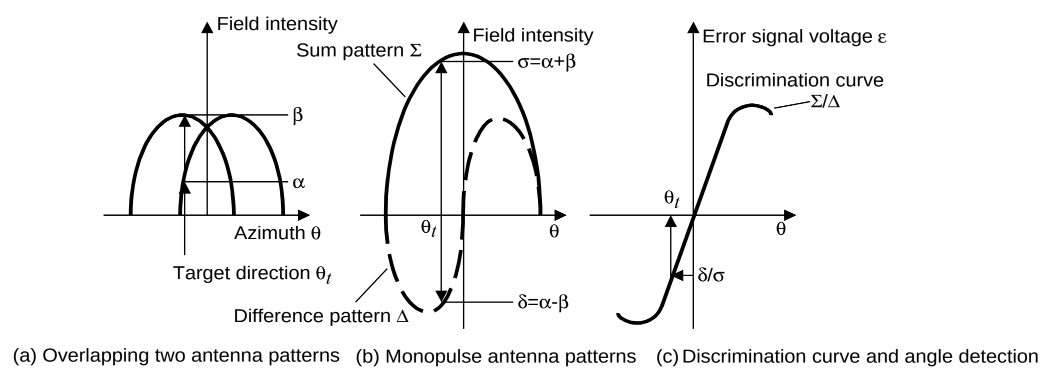

Fig. 2 Monopulse radar signal processing.

Overview of the Newly Developed Millimeter-Wave Radar

An example of the specifications of the millimeter-wave radar for automotive application is shown in Table 1. Assuming the radar is to be used in expressway driving, it must provide sufficient performance for detecting a forward vehicle at distances greater than 100m from the host vehicle. In addition, a millimeter-wave radar for automotive application must also satisfy the following requirements:

1. It must be capable of oscillating, amplifying, modulating and demodulating millimeter-wave signals stably.
2. It must be capable of radiating a millimeter-wave signal toward a target with a suitable level of power, beam width, number of beams and timing.
3. It must be capable of maintaining robust performance in the environment of the host vehicle temperature changes and vibrations.
4. Taking into account ease of installation on the host vehicle, it must be compact and lightweight.

In order to satisfy all of these requirements, Mitsubishi Electric has developed each of the elements constituting a radar head, including an RF module, antenna, antenna scanning mechanism, and radar signal-processing unit.

RF MODULE. The RF module consists of MMICs having functions such as millimeter-wave band oscillator, amplifier and mixer. The RF module also has an interface function with an antenna and a signal-processing unit. By using MMICs developed and manufactured for this automotive millimeter-wave radar, an RF module has been provided with the high output and sensitivity to achieve a maximum detection range greater than 100m. The performance stability of the RF module has been confirmed in the harsh vehicle environment.

ANTENNA. An offset paraboloidal reflector antenna is used to obtain high gain and antenna efficiency in order to provide the desired maximum detection distance and detection angle range when combined with the RF module. A reflector-rotating mechanism has been adopted that rotates only the lightweight reflector to accomplish beam scanning. One feature of this antenna is that beam scanning can be performed while the RF module is kept stationary. Another advantage is that its radiation properties show virtually no change within a beam scanning angle of ±10°.

Fig. 3 Radar head (prototype).

RADAR SIGNAL-PROCESSING UNIT. The radar system adopted combines pulse-Doppler radar with FM-CW radar. This combination reduces the rate of target detection error, which can be a problem with the FM-CW system, and thereby successfully improves target detection performance significantly. This signal-processing unit is housed in the radar head together with the RF module, antenna, reflector-rotating mechanism and power supply circuit. Fig. 3 shows a prototype radar head. The compact, lightweight radar that has been achieved is easy to install on vehicles.

A compact and lightweight millimeter-wave radar for automotive application has been developed. This radar is currently being tested under actual driving conditions as the sensor for an ACC system.❑

Technology to Integrate a Vehicle-Mounted Camera and Image-Processing Unit

*by Yoshiyuki Fujii and Hideki Tsukaoka **

The imaging camera unit and image-processing unit that were previously separate components of a camera system for lane-marking detection and preceding-vehicle recognition have been integrated by eliminating the interface circuit and incorporating the control circuit in the software. As a result, we have achieved a low-cost, substantially more compact system, 80% smaller in volume than the previous system.

Driving environment-detection and recognition technology is one of the keys to intelligent transport systems (ITS).[1] Image-processing technology, seen as a fundamental environment-sensing method, has already been implemented on some production vehicles for detecting lane markers and recognizing preceding vehicles. However, because the current image-processing system for automotive use is still very large in size and expensive, future market expansion will require a smaller and lower-cost system

Image Processing Using a Small, Inexpensive Lane-Marking Detection Sensor

An image-processing system for automotive use must be capable of detecting and recognizing target objects in real time from images taken of the driving environment. For that reason, the system hardware is more expensive than ordinary automotive sensors and is also larger. On the other hand, the locations where such a system can be installed on vehicles are generally limited for various reasons. Consequently, the imaging camera unit and image-processing unit of such systems have generally been separated in order to reduce the former's size. The configuration of a conventional image-processing system is shown in Fig. 1.[2] However, this sort of configuration has the following problems with respect to both performance and cost aspects.

- It is disadvantageous in terms of electromagnetic compatibility (EMC) because the video signals are transmitted within the vehicle.
- A filter cannot be used to secure EMC because it would attenuate the higher frequency component of the video signals.
- The use of two separate units requires duplication of structural materials, video interface, power source, timing generator and other components.

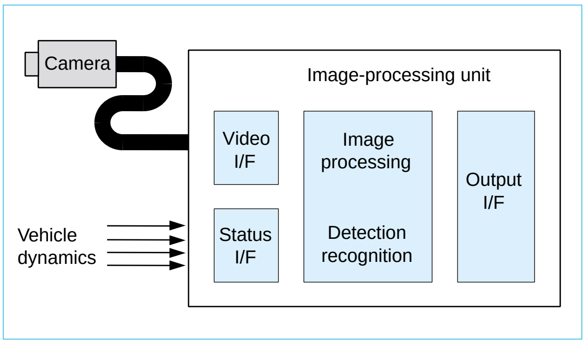

Fig. 1 Conventional image-processing system configuration

These problems can be overcome by integrating the camera and the image-processing electronic control unit (ECU). However, simply integrating these two elements would cause another problem in that the increased size of the resulting unit would make vehicle installation more difficult. Moreover, integration would also cause problems related to the increased scale of the circuit, including the issue of heat radiation associated with miniaturization, the need to develop new debugging tools and the necessity of providing a separate interface specifically for external inputs.

On the other hand, integrating the camera and image processing ECU would clearly produce large performance and cost benefits. Therefore, as the first step, we selected the dimensions of an ordinary business card as the target size of the unit, assuming that it would be installed on the back of the rearview mirror. Efforts were made to achieve size and cost reductions from three perspectives:

- Incorporation of hardware functions into the software and use of gate arrays
- Simplification of the circuitry and inputs/outputs
- Elimination of heat factors

As a result, the above-mentioned problems were resolved by adopting the improvements listed in Table 1.

Hardware Configuration of Integrated Image-Processing Camera

The part count was successfully reduced by approximately 40% by implementing the mea-

*Yoshiyuki Fujii is with the Automotive Electronics Development Center and Hideki Tsukaoka is with Mitsubishi Electric Engineering Co., Ltd.

sures noted in Table 1. Fig. 2 shows the hardware configuration of the integrated image-processing camera and its external appearance.

Images photoelectrically converted by the image sensor undergo various signal-processing operations followed by analog-to-digital conversion, after which they are written to memory via a gate array. The gate array generates various timing signals, controls external inputs and superimposes the processed results. This super-

Table 1 Miniaturization of Hardware

Item		Conventional methods	Integration	Effect
ECU	Video I/F	EMI filter	Delete	Miniaturization
		Sync. separator	Delete	
		PLL	Delete	
		SSG	Delete	
		Video amp	Delete	
	Vehicle status	SCI	CAN	
	Pre-processing	Hardware	Software	
	Power supply	Series regulator	DC/DC converter	Heat reduction
Camera	CCD	1/3rd inch	1/4th inch	Miniaturization
	Iris	Mechanical	Electronic	
	Iris control	Hardware	Software	
	AGC			
	Camera control			

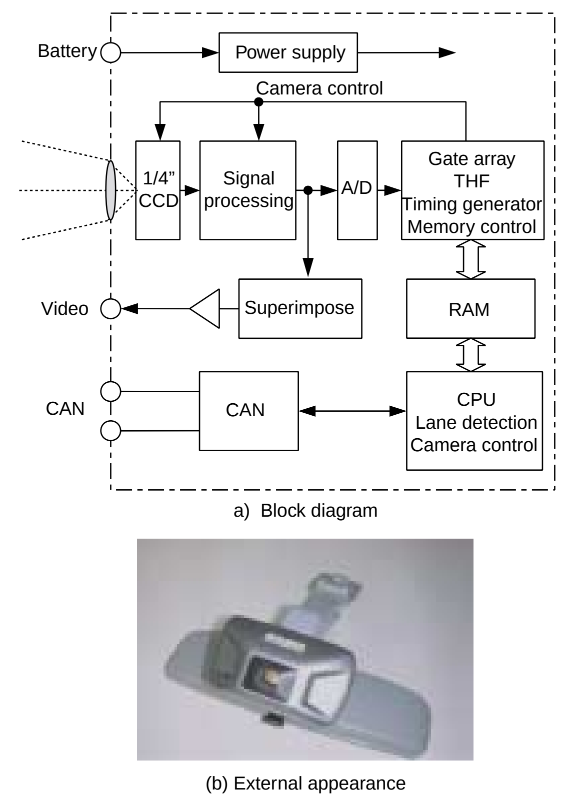

a) Block diagram

(b) External appearance

Fig. 2 Image-processing camera

imposition function is extremely effective for theoretical software debugging. An inexpensive gate array with fewer gates was adopted by having the software pre-process the images, which simultaneously achieved a cost reduction. The CPU performs lane detection and preceding-vehicle recognition based on the images written to memory and information on the host vehicle's dynamic status, and the result is output via the controller area network (CAN). The CPU also controls the camera exposure and camera characteristics. The various operating parameters of the camera require no adjustment, which simplifies the manufacture of the camera and also reduces its cost.

Lane-Detection Method

The performance of the lane-detection function is greatly affected by the weather and the ambient environment. However, white-line lane markers on an asphalt road surface are basically characterized as having a higher degree of luminance than that of the surrounding road surface. The top-hat filter (THF) is an image filter that focuses on this characteristic. Letting C, L and R denote the respective horizontal coordinates and h the width of a white line in an image captured with the image sensor, the THF value at point C is given by the following equation:

$$\text{THF}(C) = \min\{\text{Lum}(C) - \text{Lum}(L),\ \text{Lum}(C) - \text{Lum}(R)\} \quad \text{............ Eq. (1)}$$

where $L = C - h$ and $R = C + h$ and Lum (x) is the luminance at point x. Eq. (1) shows that bright points having a width smaller than h can be extracted without being influenced by the changing luminance of the surroundings. Using this computational method, white-line lane markers can be detected with a simple algorithm. This effect of THF is shown in Fig. 3.

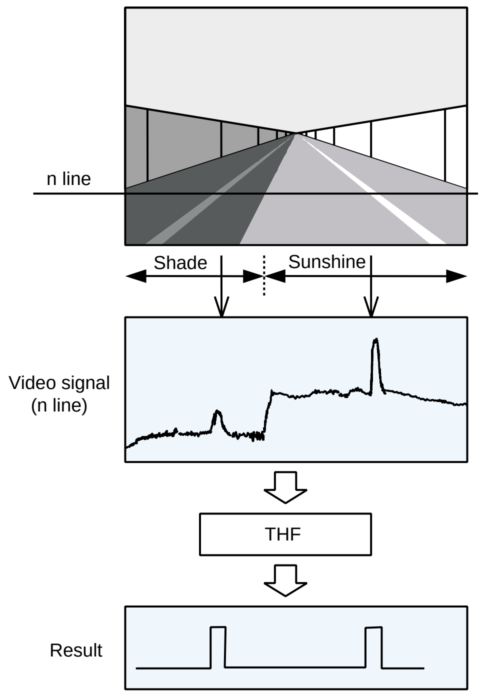

Fig. 3 The effect of a THF

Vehicle-Recognition Method

In general, it is extremely difficult to extract the complex features of a detected object, such as a preceding vehicle or an obstacle, under the limitations of a simple hardware configuration and real-time processing. The camera we have developed does not focus on the features of a vehicle, but rather it detects "objects that are not the road surface" based on changes in the road surface luminance. An example of the vehicle recognition results is shown in Fig. 4.

Fig. 4 Vehicle detection

Yellow-Line Detection Method

Ordinarily, yellow lines tend to be lost very easily because it is difficult to obtain a difference in luminance between them and the road surface. This problem has been resolved by adopting an optical filter specifically for yellow-line detection, focusing on the differences in spectral characteristics between yellow lines and asphalt. The use of this filter makes it possible to detect yellow lines with the same algorithm as that used for white lines. The effect of this filter is shown in Fig. 5.

(a) Without filter

(b) With filter

Fig. 5 The effect of a filter for yellow-line detection

Specifications of Integrated Image-Processing Camera

The specifications of the newly developed camera with an integrated image-processing unit are given in Table 2. This camera is not only applicable for monitoring the environment ahead, it can also be used for monitoring all around a vehicle, including the rear, lateral and oblique rear directions, by changing the software.

Table 2 Image-Processing Camera Specifications

Image sensor	1/4-inch B&W CCD
Effective pixels (H x W)	510 x 492
Lens	6mm/F4, field of view 33° (H)
Auto-level control	Electronic iris, AGC, selected area metering
Signal-to-noise ratio	Better than 45dB (AGC off)
Detecting area	~50m at 26° (height 1.3m)
Optical axial aberration	Auto calibration and learning
Input/output	CAN, SCI
Video output	EIA $1V_{p-p}$ (Detection results can be superimposed)
Power supply	DC, 8~32V (less than 3W)
Overall dimensions (W x H x D)	105 x 62 x 44.8mm
Weight	Less than 0.3kg
Operating temperature range	–30° ~ +90°C
Storage temperature range	–30° ~ +80°C

There are strong automotive industry needs for image-processing sensors capable of recognizing the driving environment, because such a sensing device is an essential component in configuring various types of in-vehicle systems. Along with the penetration of ITS technologies in the coming years, these sensors are expected to find widespread use. In future work, we intend to pursue further size and cost reductions and to improve robust detection performance. ❑

References

[1] Shin-ichi Sato, Yuhei Akasu, Kazumichi Tsutsumi and Yoshiaki Asayama, “Key ITS In-vehicle Technologies,” Mitsubishi Electric Technical Review, Vol. 73, No. 10, pp. 17-11 (1999).

[2] Kazumichi Tsutsumi, Yuhei Akasu, Kazuhiro Ikebuchi, Shigekazu Muraoka, Hiromichi Kushizaki and Minoru Nishida, “Headway Distance Control Technology,” Mitsubishi Electric Technical Review, Vol. 70, No. 9, pp. 13-16 (1996).

Static Steering-Control System for Electric-Power Steering

*by Masahiko Kurishige and Takayuki Kifuku**

Electric-power steering (EPS) systems have attracted much attention for their advantages with respect to improved fuel economy and have been widely adopted as automotive power-steering equipment in recent years. The article introduces a new EPS control system that reduces steering torque during static steering (i.e., while a vehicle is at rest) as a means of further improving EPS control performance.

Required Control Performance During Static Steering

An EPS system controls the current of a motor to generate assist torque based on the output of a steering-torque sensor. The assist torque is set so that it is nearly proportional to the sensor output. Increasing this proportional gain (i.e., map gain) has the effect of reducing steering torque, but in the vicinity of 30Hz the control system may oscillate, causing a driver to feel unpleasant steering-wheel vibration. In general, drivers tend to prefer a low level of steering torque during static steering. Accordingly, the challenge is to suppress steering-wheel vibration while at the same time reducing steering torque.

Damping Control System Design Incorporating an Observer

Fig. 1 shows a model of a steering mechanism equipped with EPS. We linearize this model and perform frequency analysis[1] to elucidate the oscillation mechanism during static steering. As shown in Eq. (1), this model can be represented as a balance between the motor inertia, the steering torque applied by the driver T_{hdl}, the assist torque produced by the motor T_{ASSIST} and the reaction torque of the steering mechanism T_{tran}. During static steering, the area of contact between the front tires and the road surface does not change in the region of small steering-wheel angles. Since the torsion of the tires acts as a spring, the steering angle and reaction torque have a proportional relationship with nearly constant gain.

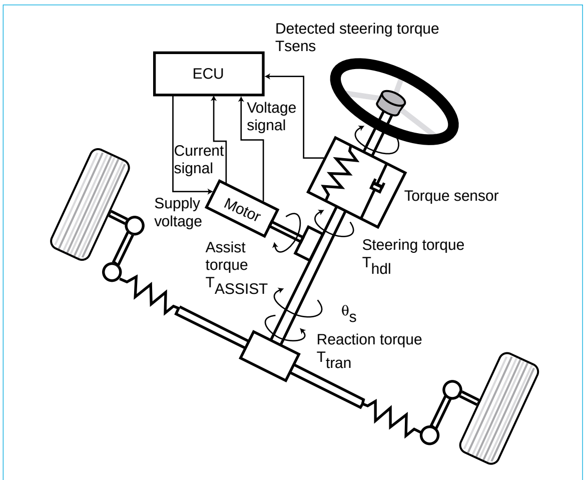

Fig. 1 A steering mechanism with EPS.

$$J \cdot d^2\theta s/dt^2 = T_{ASSIST} + T_{hdl} - T_{tran} \quad \text{Eq. 1a}$$

$$T_{ASSIST} = G_{gear}\{K_T \cdot I_{mtr} - T_{fric} \cdot \mathrm{sgn}(d\theta_s/dt)\} \quad \text{Eq.1b}$$

$$T_{hdl} = K_{TSEN}(\theta_{hdl} - \theta_s) + C_{TSEN}(d\theta_{hdl}/dt - d\theta_s/dt) \quad \text{Eq.1c}$$

where

- K_T motor-torque constant
- I_{mtr} motor current
- T_{fric} motor-friction torque
- K_{TSEN} spring constant of the torque sensor
- C_{TSEN} damping coefficient of the torque sensor
- θ_s angle of steering-column shaft
- θ_{hdl} steering-wheel angle
- G_{gear} motor-gear ratio
- J motor moment of inertia

The calculated frequency characteristics of the linearized model are shown by the solid lines in Fig. 2. The control system has been designed with a phase margin in the vicinity of the crossover frequency where the gain is 0dB. However, when the map gain is increased, the crossover frequency shifts to the high frequency side and the phase margin decreases, which tends to induce control-system oscillation.

An effective way of suppressing steering-wheel vibration is to incorporate a control measure that applies damping at the frequency where oscillation occurs, but an EPS system does not have a motor-speed sensor. Previously, the motor speed has been estimated in the low-fre-

Masahiko Kurishige is with the Industrial Electronics & Systems Laboratory, and Takayuki Kifuku is with Himeji Works.

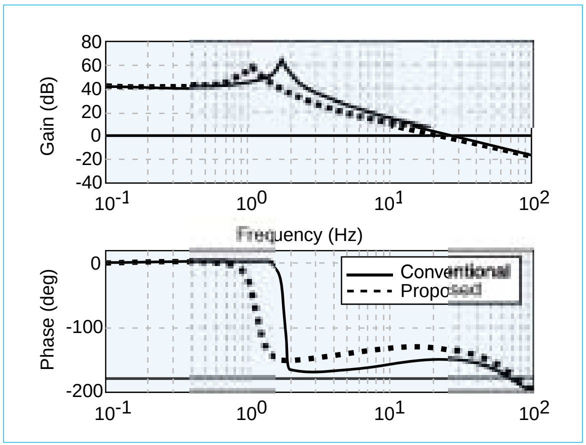

Fig. 2 Frequency characteristics of a steering mechanism with EPS.

quency region below 5Hz, but it has been difficult to estimate the motor speed in the vicinity of an oscillation frequency of 30Hz.

To overcome this problem, we have devised a method of estimating the motor speed by using an observer[2] and have developed a damping compensator that provides compensation based on the estimated motor-speed signal. This has resulted in comfortable static steering performance free of steering-wheel vibration.

The configuration of the observer is described next. This observer has been constructed by linearizing the model in Eq. 1, and has the steering torque and motor current as its inputs. To validate the operation and estimation performance of the observer, an estimate was made of the motor speed when static steering oscillation occurred. The results are shown in Fig. 3

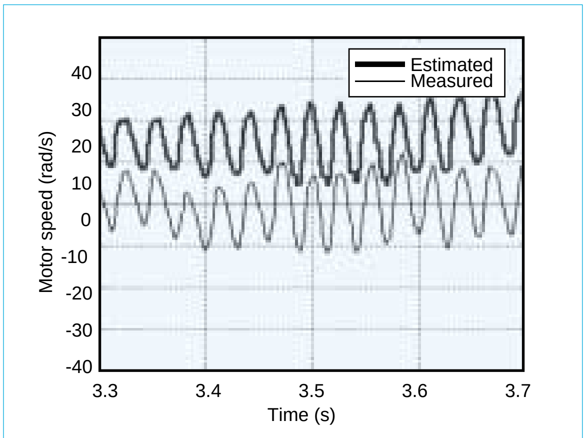

Fig. 3 Estimation of motor speed using an observer.

where the thicker line indicates the motor speed measured with a rotary encoder and the fine line shows the speed estimated by the observer. The estimated results agree well with the measured data in terms of both the amplitude and phase of the motor speed.

The input signal is filtered with the aim of applying damping only at the frequency where steering system oscillation occurs, so the estimated motor speed fluctuates near a value of zero. Therefore, when oscillation damping control is performed based on the motor speed estimated by this observer, there is no feedback of the steering velocity component. Accordingly, since damping control does not manifest itself as steering resistance, it is possible to achieve comfortable steering behavior.

A block diagram of the new controller that performs feedback of the estimated motor speed is shown in Fig. 4, and its frequency characteristics are indicated by the dashed lines in Fig. 2. Although the phase margin is larger than that of the previous system, the control system is not affected by high-frequency mechanical resonance because the high-frequency gain does not change.

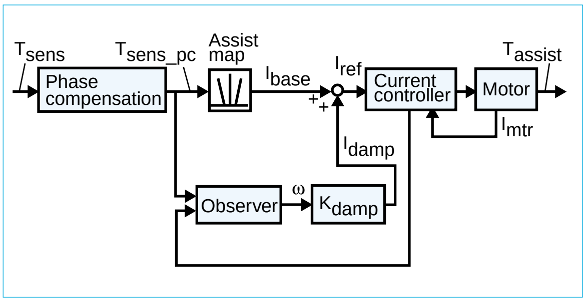

Fig. 4 Block diagram of the contoller with damping compensation.

Vehicle testing

To verify the performance of the proposed controller, tests were conducted with an actual vehicle using the DSP-CIT controller development tool that is capable of generating a control program seamlessly from the controller model constructed with MATLAB/SIMULINK. The map gain was increased 3.3-fold over the conventional level. While oscillation occurred with the conventional controller, see Fig. 5 (a), no oscillation occurred with the proposed controller, Fig. 5 (b). These

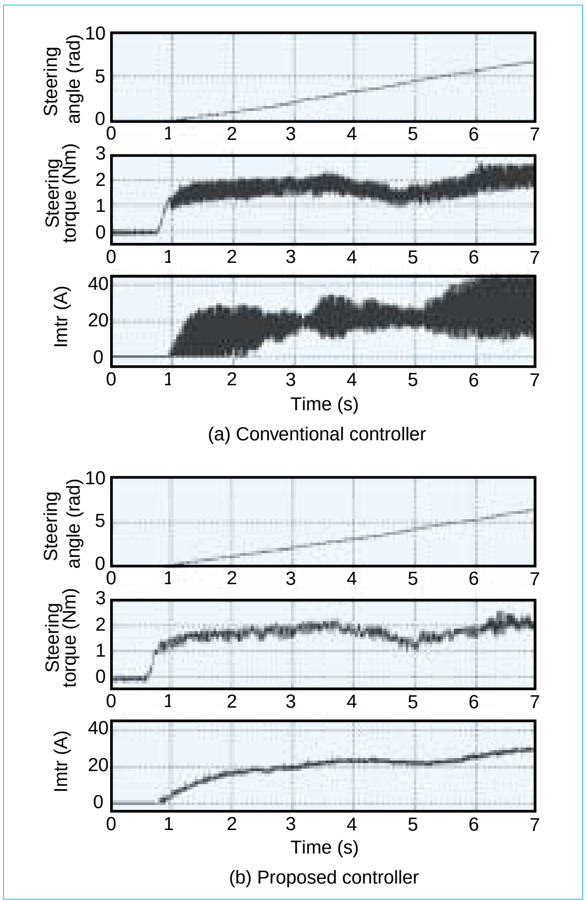

Fig. 5 Experimental results with conventional and proposed controllers.

results confirm that the application of an observer and damping control to the EPS control system have improved static steering performance.

In future work, efforts will be made to apply this control system to a high-output motor and to improve the control performance further. Technologies will be developed for applying EPS widely to small and midsize cars with the aim of contributing to the further development of such vehicles. ❑

References

1. M. Kurishige, et al., "A Control Strategy to Reduce Steering Torque for Stationary Vehicles Equipped with EPS," SAE Paper No. 1999-01-0403 (1999).
2. D. G. Luenberger, "Observing the state of linear system," IEEE Trans. Mil. Electron, MIL-8, 74-80 (1964).

Development of Car Navigation Software

*by Toshiki Kusama and Akio Uekawa**

Continuing progress in car navigation systems is rapidly increasing the cost and time needed to develop the associated software. To ease this problem, we have developed a car navigation software development framework called Victoria that substantially improves software productivity. The effectiveness of this framework has been confirmed and is described here together with an overview of Victoria.

The Victoria Approach

The cost and time required for software development, including the extension of specifications when a new model is created and the cost and time needed to make modifications, are expressed by the following equation.

Development cost and time = cost and time required to clarify specifications + the amount of modification work/work done per unit time

The following approach has been devised to reduce software development cost and time.

REDUCTION OF COST AND TIME REQUIRED TO CLARIFY SPECIFICATIONS. The process of making ambiguous specification requirements, including the specifications demanded by the customer and others, into rigorously defined specifications is a major and vitally important undertaking. A human-machine prototyping tool was developed and implemented to make it easy to determine the specifications of ill-defined user interfaces, which are responsible for the most specification changes in the entire system.

REDUCTION OF MODIFICATION WORK. The software was redesigned to localize modifications resulting from specification changes and to reduce the amount of modification work required. This involved separating the elements dependent on the human-machine interface specifications, the database-dependent elements and the platform-dependent elements. Additionally, an object-oriented language was used to develop the framework in order to localize the places requiring modification and improve extensibility.

IMPROVEMENT OF WORK DONE PER UNIT TIME. The conventional development environment for embedded systems is referred to as a cross-development environment in which a host computer and the target hardware are connected to carry out the development work. The newly developed framework has a middleware layer that absorbs differences between the development environment on the target hardware and the development environment on a PC. This facilitates the sharing of higher level car-navigation software and enables the development work to be done on a PC.

An automatic software generator based on a human-machine builder was also developed to boost the development efficiency of the user interface element, which requires the largest number of modifications on each model.

Object-Oriented Development

C++ was adopted as the object-oriented language, and the software architecture was restructured to minimize the amount of software modifications needed to effect specification changes. This was done to reduce linkage between modules and to localize modifications.

Development in a PC Environment

A middleware layer is provided to absorb development environment differences between the target hardware and a PC, allowing higher level car-navigation software to be shared.

The higher level software does not issue a system call directly to the operating system (OS) but rather through the middleware. The middleware for the target hardware environment and that for the PC environment are interchangeable, facilitating software development on a PC.

Developing the software on a PC makes it possible to utilize the outstanding development environment available for PCs. Because the entire process from software development to system testing and improvement can be done on the same PC, the debugging cycle can be shortened.

Fig. 1 shows an example of the development environment on a PC. Operations can be executed via input from keyboard or mouse. A dia-

**Toshiki Kusama is with Sanda Works and Akio Uekawa is with the Energy & Industrial Systems Center.*

Fig. 1 The development environment on a PC.

log box is provided to reproduce sensor data, such as the signals of the global positioning system (GPS), gyro and vehicle-speed pulses, and vehicle information and communication system (VICS) data. It is also possible to simulate driving operations and reception of VICS data. At the final stage of development, the middleware can be substituted for that of the target hardware environment, as shown in Fig. 2, and a cross-compiler can be developed in the target hardware environment. Microsoft's Windows NT4.0 has been adopted as the OS of the PC environment and Microsoft's Windows CE as the OS of the target hardware environment.

Separation of Map Database-Dependent Part by Using a Map API

Map databases for car navigation systems have yet to be unified, and each company currently uses its own map format. Previously, we devel-

Fig. 2 The development environment on target hardware.

oped car-navigation software separately for each company's format, as shown in Fig. 3. To avoid duplication of development work for each format, we separated the map database-dependent part as a map-access library and specified a map application program interface (API) as the programming interface for map access.

As shown in Fig. 4, the higher level software accesses maps in each format via the map API, making the software independent of the map format and allowing common usage.

Software Development Using a Human-Machine Builder

The elements dependent on the human-machine specifications were separated and a prototyping tool was adopted to support specification decisions and a human-machine builder was applied

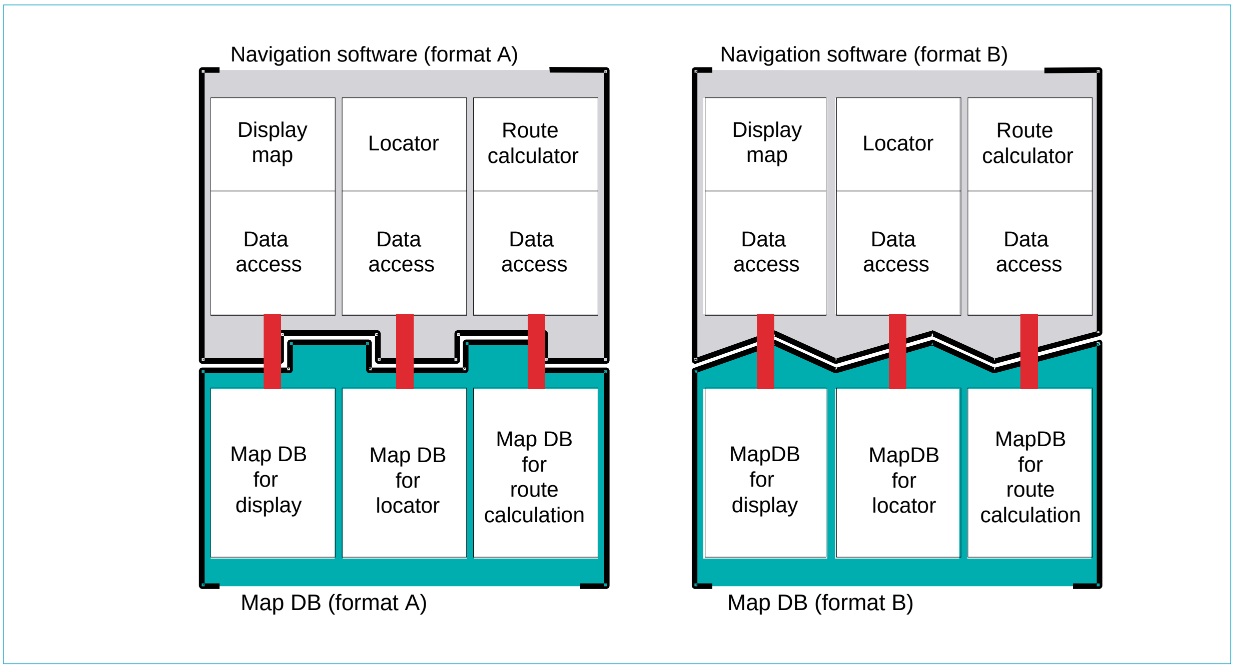

Fig. 3 Conventional access to map database

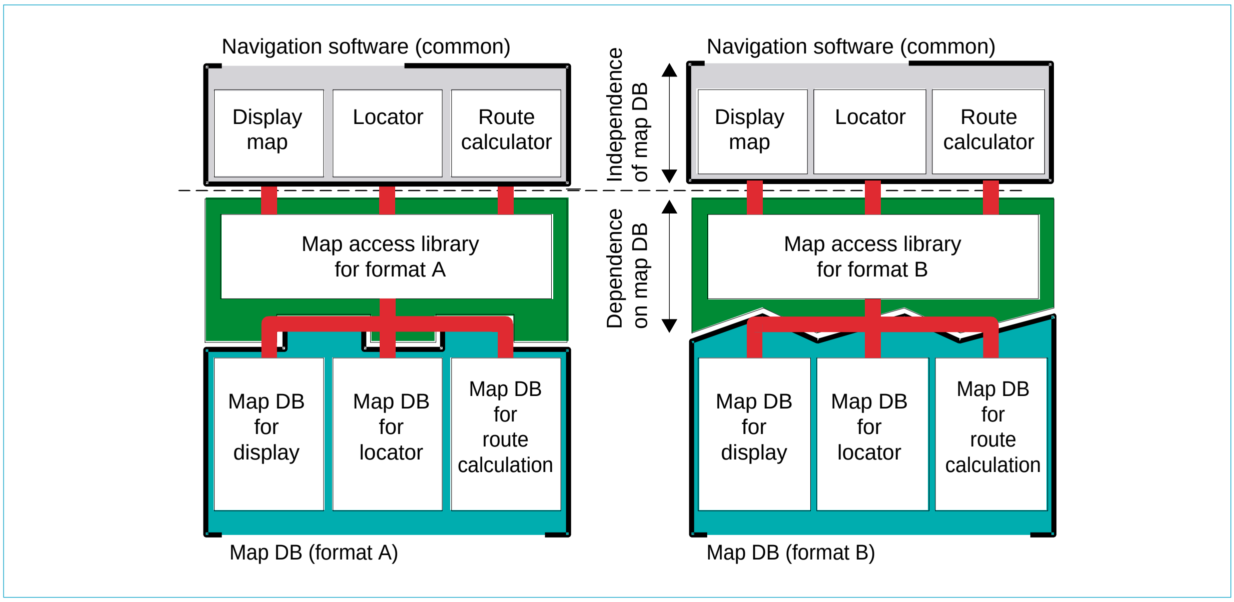

Fig. 4 Access to map database through map API

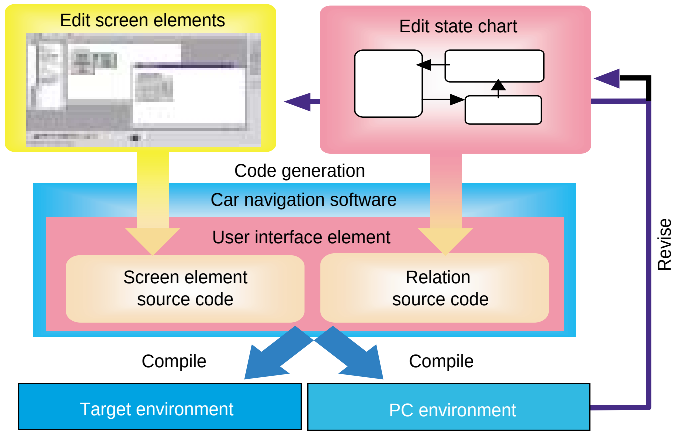

Fig. 5 Development user-interface element using the human-machine builder

to the automatic software generator for the user interface element. The human-machine builder makes it easy to modify the areas of the software that have to be revised. It also minimizes duplicated effort because consistent support is provided from the upstream design process where the human-machine specifications are examined.

As shown in Fig. 5, the map screens of a car navigation system are created with a screen editor and the operational transitions and actions are described in state transition diagrams. Thanks to the use of an automatic code generator, the screen parts and actions thus created become the source code that can be run as it is on the PC environment and the target hardware environment. The entire cycle from confirmation of an action to its modification can be executed on the same PC. The screen editor is a tool that we have newly developed for creating car navigation system screens and can be used in the same way as an ordinary drawing tool. A commercially available tool is used to describe the state transition diagrams.

The new software support framework promises to increase the speed and flexibility with which Mitsubishi Electric can accommodate the rapidly increasing complexity and sophistication of car navigation systems. ❑

Powertrain Control-System Development Support

*by Jiro Sumitani and Kiyoharu Anzai**

Today's automotive powertrain control systems must meet a wide variety of performance requirements, from improving the necessary inherent vehicle performance to satisfying demands for lower fuel consumption, cleaner exhaust emissions and improved safety. Control-system specifications have thus become extremely complex. The article presents an overview of a powertrain control-system development support environment created to facilitate more efficient development of optimum control systems.

Powertrain Control-System Development Characteristics and Issues

An automotive powertrain control system is typically developed through a repeated process of identifying and resolving problems based on actual vehicle tests until the desired performance is attained. The flow of this development process is shown in Fig. 1.

Global environmental concerns and other factors today mean that the specifications of a powertrain control system must meet a widening range of performance requirements. As a result, the control specifications have become more complex and require much greater development time and expense. However, because of intensifying global competition, the development lead time of vehicles must be shortened. Accordingly, more efficient development of powertrain control systems is a high priority.

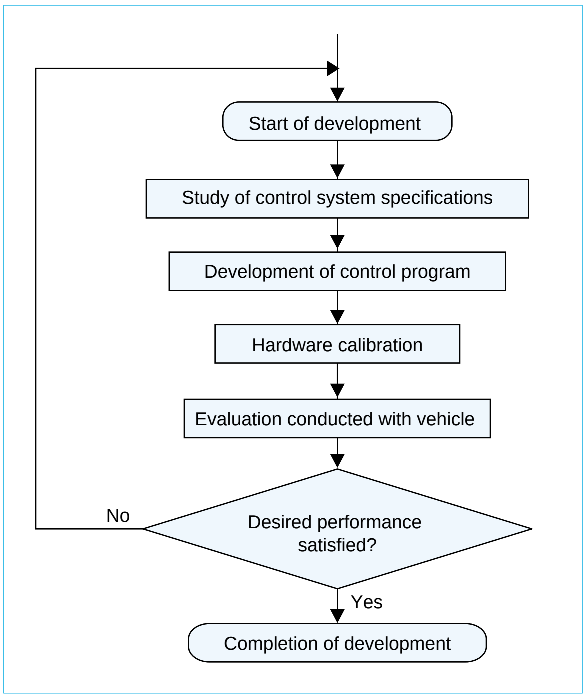

Fig. 1. Development flow for a powertrain control system.

Development Measures Incorporated in the Support Environment (see Fig. 2)

IMPROVING THE DEVELOPMENT PROCESS. Accelerating the study of control-system specifications is one such important improvement. Simulations are conducted based on control-model diagrams created with commercially available control-system design tools and programs can now be generated automatically, as will be described below. These measures enable theoretical studies of control-system specifications and actual vehicle tests to be conducted more efficiently.

AUTOMATING HARDWARE CALIBRATION. A powertrain control system contains numerous control parameters generally set according to calibrations based on tests conducted with the actual vehicle. An automatic calibration envi-

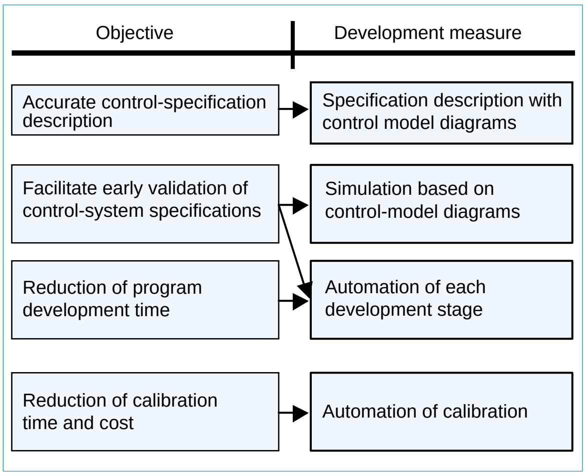

Fig. 2. Development measures incorporated in development support environment.

*Jiro Sumitani is with Himeji Works and Kiyoharu Anzai is with Mitsubishi Electric Control Software Corp.

ronment has been developed to improve development efficiency.

Improved Software Development.

AUTOMATIC SOFTWARE GENERATION. If the control program could be generated automatically from the control-model diagrams that represent the control-system specifications, development efficiency would be substantially improved. Automatic program generation itself is possible today through the use of commercially available tools. However, with just the standard functions of the commercial tools currently available, there are some problems in the description of data processing. The development support environment was therefore created to supplement the capabilities of commercially available tools.

AUTOMATIC DOCUMENT GENERATION. The procedure usually followed in developing a powertrain control system is to make improvements on the basis of repeated tests conducted with the actual vehicle. Such tests require detailed control-system specification documents covering control parameters and control variables. These documents must be created concurrently with the control program every time tests are conducted. An environment has been constructed that generates control-system specification documents automatically from control-model diagrams and other information so as to improve development efficiency.

ALICE Development Support Environment

The advanced logic integrator for car electronics (ALICE) environment (see Fig. 3) has been developed for powertrain control-system development. ALICE is built around MATLAB/Simulink (from The MathWorks, Inc.), a commercially available control-system design support tool, and the TargetLink code generator (from dSPACE GmbH) that runs on MATLAB and generates fixed-point program code. To these core capabilities we have added the above-mentioned unique functions developed by Mitsubishi Electric Corporation.

ALICE Workbench

This is an integration tool built to enable various development support tools created in-house to be used with consistent operating procedures. These tools include ALICE Designer, which incorporates additional functions for specification descriptions based on control-model diagrams, for comparing control-model diagrams and for conducting information searches. It improves the development efficiency and reliability of control-model diagrams using the ALICE Auto Coder that automatically generates optimized object code based on control-model diagrams; the

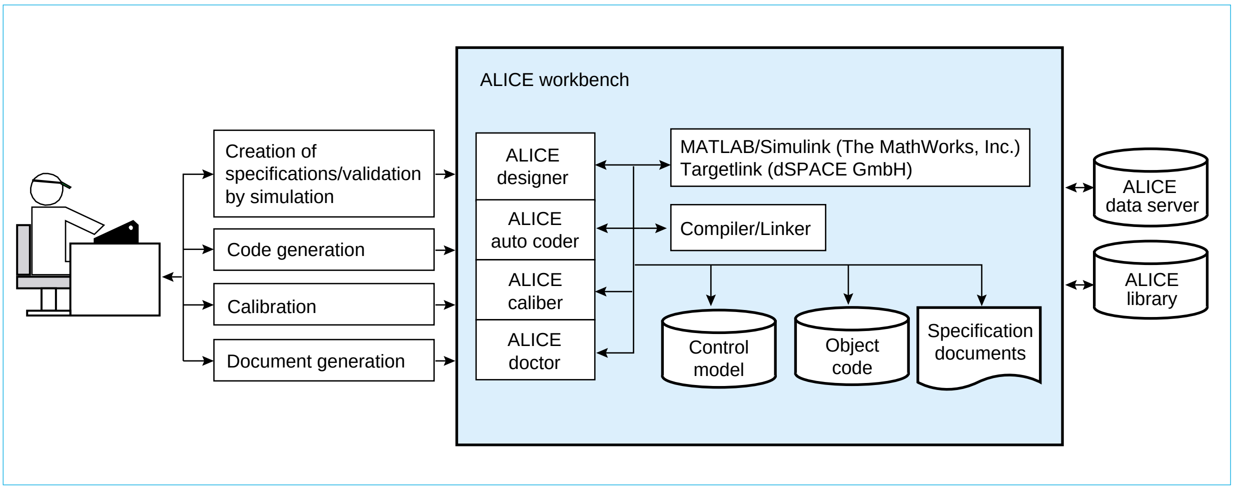

Fig. 3. ALICE development environment.

ALICE Doctor (document generator) that automatically generates detailed specification documents from control-model diagrams and other information; and the ALICE Caliber that automatically generates the information for calibrating the actual powertrain hardware.

ALICE Data Server

A control model generally describes the processing operation in terms of actual physical quantities. However, functional limitations of the microcomputer that is used require conversion to a fixed-point processing description. Conversion to a fixed-point description can be accomplished with TargetLink, but the various types of information required must be entered manually in each mathematical function block. Therefore, an environment has been created that facilitates automatic entry all at one time through centralized management of the information needed for conversion to a fixed-point description.

ALICE Library

It is difficult to describe interrupts and the like with just the standard control-model description blocks of MATLAB. To make such descriptions possible and reduce the size of the program that is generated, we created an independent block for powertrain-control descriptions and incorporated it into the ALICE Library.

Development of an Automatic Calibration Environment

Calibration has traditionally been performed as shown in Fig. 4. Control parameters were changed manually and measured for each operating state of an actual vehicle, and the process of changing the parameters was repeated until the measured results coincided with the target control values. One problem with this approach has been the enormous time and cost involved in processing the data.

To resolve this problem, input/output functions for controlling the operating state of the actual vehicle were added to the previously used calibration tool along with an automatic processing capability, as shown in Fig. 5. This resulted in the creation of an automatic-calibration environment configured as shown in the diagram.

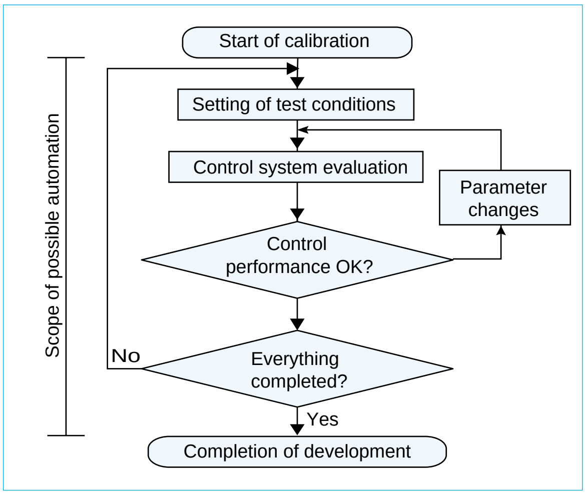

Fig. 4. Conventional calibration procedure

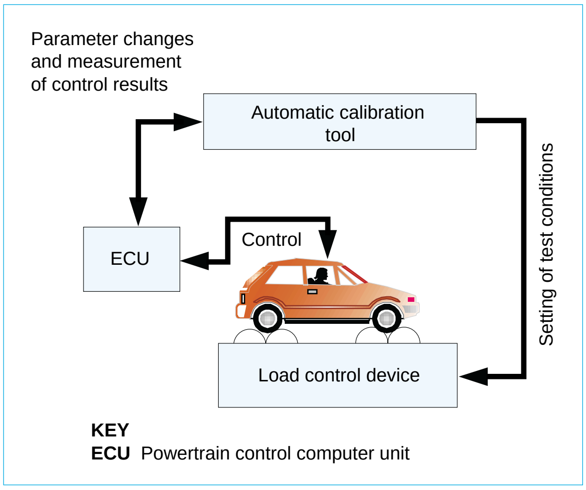

Fig. 5. System configuration of automatic calibration environment

The article presents the overview of an environment created to support more efficient development of complicated powertrain control systems. The use of this environment and associated tools makes it possible to improve overall efficiency, from the initial study of the control-system specifications through to vehicle calibration. Through our work of developing car electronics, we intend to contribute to the future development of the automotive industry. ❑

Digital Signal Processing Technology for Car Radios

*by Masahiro Tsujishita and Eiji Asano**

In order to improve performance and reduce the component count of an AM/FM car radio receiver, we have converted it to digital operation. The article describes the system configuration and the signal-processing technology.

Development of a Digital FM radio

A block diagram of the newly developed digital AM/FM radio receiver is shown in Fig. 1. The system mainly consists of an AM/FM front-end, limiter, mixer and digital signal processor. As shown in Fig. 2, the digital signal processor performs the tasks of FM demodulation, multipath noise reduction, pilot synchronization, stereo demodulation and pulse-noise reduction. An explanation follows of the method adopted to reduce FM demodulation distortion and the processing procedure to reduce external noise, both characteristic features of the newly developed digital signal processing technology.

Improving Digital FM Demodulation Distortion

CORRECTION OF IF SIGNAL-AMPLITUDE VARIATION. The bandwidth limit of the low-pass filter placed before the A/D signal converter causes the carrier amplitude of an FM signal to vary. FM demodulation of the signal under these conditions generates distortion. To eliminate this distortion, the amplitude compensator detects the carrier amplitude X and multiplies the output signal of the FM demodulator by 1/X, as shown in Fig. 3. With the newly developed digital signal processing technology, this amplitude correction achieves a distortion of less than 1% (for 30% modulation at 1kHz) while allowing the cut-off frequency of the forward low-pass filter to deviate by ±20%.

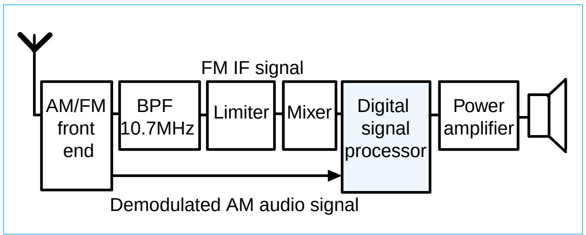

Fig. 1 Block diagram of an AM/FM receiver

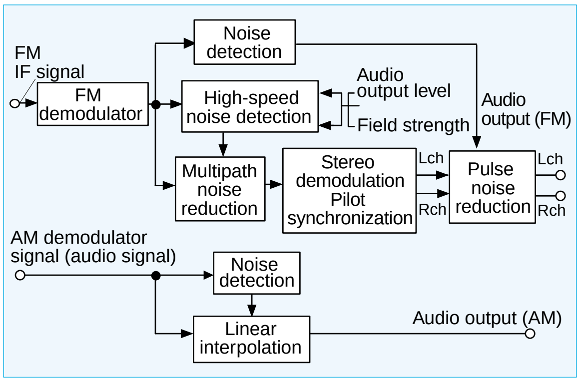

Fig.2 Block diagram of digital signal processing

IMPROVEMENT OF DIGITAL FM DEMODULATION DISTORTION. In the arc-sine compensator in Fig. 3, an approximation of the arc-sine curve is used to correct the distortion caused by the static characteristic of the sine curve generated by the quadrature FM demodulator. This has the effect of reducing the distortion by about 10dB for 100% modulation.

Improved Noise Reduction

For good radio reception in the automotive environment, it is necessary to reduce pulse noise caused by electromagnetic wave noise and multipath noise caused by signal reflection from mountains and man-made structures.

REDUCING FM RECEIVER PULSE NOISE. This newly developed signal processing technology suitably switches between interpolation methods depending on the frequency components of the FM stereo demodulated signal. Moreover,

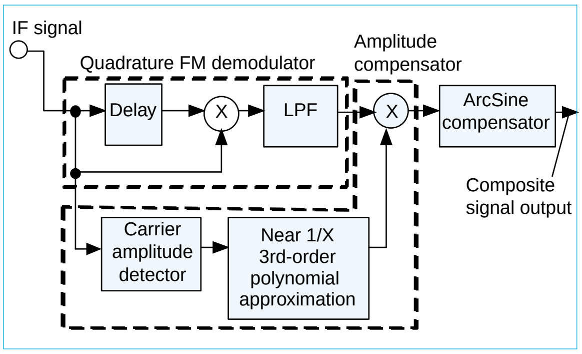

Fig. 3 Block diagram of FM demodulation

**Masahiro Tsujishita is with the Imaging Systems Laboratory and Eiji Asano is with Sanda Works.*

as shown in Fig. 2, the L-channel and R-channel signals are corrected separately following stereo demodulation. This approach is especially effective in reducing high pulse noise in stereo-signal reception. The signal waveforms before and after interpolation are compared in Fig. 4.

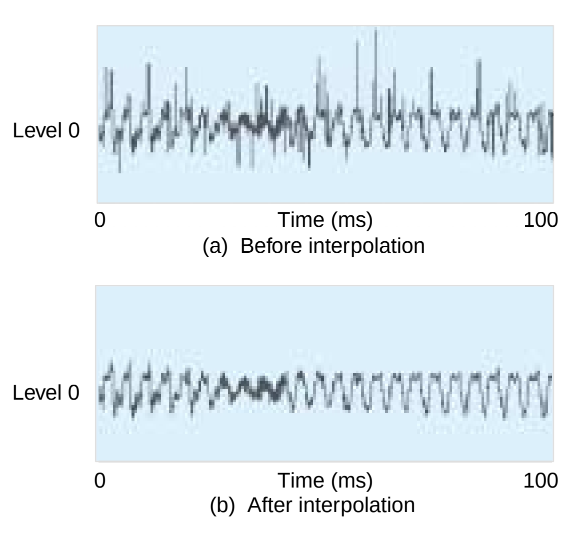

Fig. 4 The effect of pulse-noise reduction (FM)

REDUCING MULTIPATH NOISE. All of the spiky noise lasting several μs that arise in the FM demodulated signal are processed one by one with this new technology to maintain the original signal values. This procedure is highly effective in reducing multipath noise. The signal waveforms before and after interpolation are compared in Fig. 5.

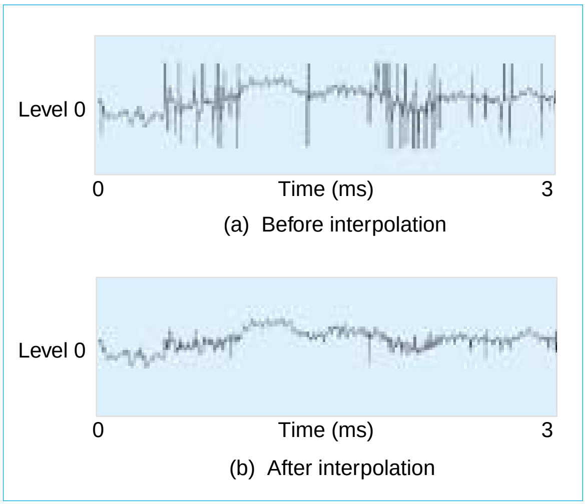

Fig. 5 The effect of multipath noise reduction

REDUCING AM RECEIVER PULSE NOISE. As shown in Fig. 2, reduction of AM receiver pulse noise involves detection and interpolation of noise components in the AM demodulated signal. Noise correction is performed by linear interpolation, whereby the correction interval is adapted to match the noise occurrence interval and pulse height. This approach is highly effective in reducing pulse noise. The signal waveforms before and after interpolation are compared in Fig. 6.

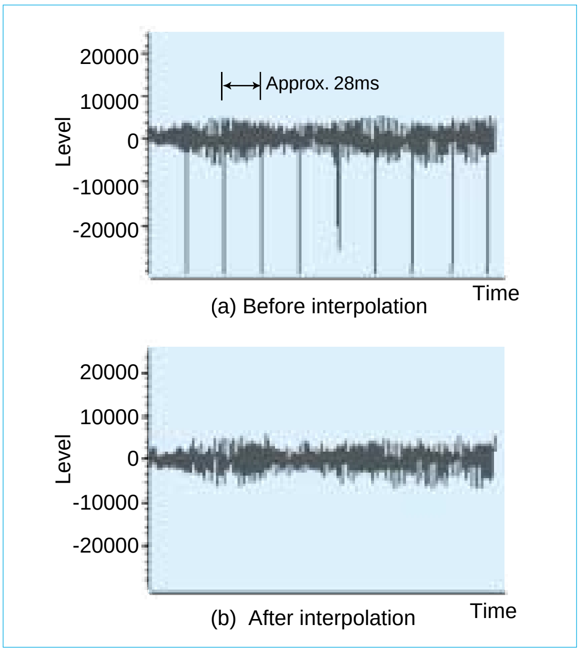

Fig. 6 The effect of pulse noise reduction (AM)

For current FM broadcasts, the newly developed digital receiver can handle the signal from the IF stage right to the audio signal. An adaptive signal processing technology using a digital signal processor has been adopted that provides a greater noise reduction effect for both AM and FM broadcasts than the analog system it will replace. ❑